J. Hydrol. Hydromech., 73, 2025, 2, 132–142
https://doi.org/10.2478/johh-2025-0010

sciendo Journal of Hydrology and Hydromechanics Institute of Hydrology SAS

Free flow over a partially contracted thin-plate weir with a triangular notch of angle 20.23° and zero weir height

Šimon Pospíšilík[1], Stanislav Kotaška[1*], David Duchan[1], Zbyněk Zachoval[1], Martin Orfánus[2], Andrej Šoltész[2], Andrzej Tadeusz Gruchot[3], Tymoteusz Zydroń[3]

[1] Brno University of Technology, Faculty of Civil Engineering, Institute of Water Structures, Veveří 331/95, 602 00 Brno, Czech Republic.
[2] Slovak University of Technology, Faculty of Civil Engineering, Department of Hydraulic Engineering, Radlinského 11, 810 05 Bratislava, Slovak Republic.
[3] University of Agriculture in Krakow, Faculty of Environmental Engineering and Geodesy, Department of Hydraulic Engineering and Geotechnics, Adama Mickiewicza 24/28, 30-059 Kraków, Poland.
[*] Corresponding author. E-mail: stanislav.kotaska@vut.cz

Abstract: The paper explores flow characteristics in the case of free flow of clean water over a partially contracted thin-plate weir with a triangular notch of angle 20.23° and with zero weir height above the bottom of the approach channel of rectangular cross-section at 5 approach channel widths and 7 heads. The description was based on the results from experimental research and numerical simulations. The numerical simulations allowed the description of the characteristics in parts of the flow where measurements were difficult to perform. The experimental research quantifies the validity of the numerical simulations and establish recommendations for construction of numerical models. The boundary between a partially contracted weir and a fully contracted weir was established by dimensionless approach channel width of the value 0.32, the flow characteristics (water surface, velocity) in the full range of the partially contracted weir (dimensionless approach channel width in range $0.32 \leq B_U^* \leq 1.00$), and recommendations for the placement of a cross-section to measure water surface level for determine the heads (dimensionless distance $-4 \leq x^* \leq -2$) were verified.

Keywords: Triangular-notch (V-notch) thin-plate weir; Free overflow; Experimental research; Numerical simulations; Partially contracted weir.

1 INTRODUCTION

Weirs are widely used in water management, mainly for rise the water surface level and for discharge measurement (Bos, 1989). Thin-plate weirs (TPWs) (also called sharp-crested weirs (Hager, 2010; Subramanya, 2009) are mainly used for relatively accurate determination of discharge of relatively clean water. TPWs are defined by the length of the weir crest in the direction of flow ranging from 0.001 m to 0.002 m (ISO, 2017). TPWs with a triangular notch (also referred to as V-notch (Milburn and Burney, 1988) or triangular weir (Hager, 2010)) are particularly suited for measuring small discharges where the use of TPWs with other notch shapes (rectangular, trapezoidal, etc.) is not appropriate. To ensure relatively accurate discharge measurement, they require that the triangular notch is placed perpendicular to the sides and bottom of a straight approach channel. The line which bisects the angle of the notch should be vertical and at the same distance from both sides of the approach channel (Bos, 1989). For relatively accurate measurements, the approach channel requirements must also be met. The approach channel must simulate normal (approximately uniform flow) conditions of flow in a smooth, horizontal and straight channel with rectangular cross-section (Shen, 1981).

The flow over TPWs with a triangular notch is significantly influenced by the weir height and the approach channel width. The approach channel width primarily influences the formation of the side wakes (or separation zones with recirculation of flow), which form immediately upstream of the weir plate near the sidewalls of the approach channel. The relative proximity of the side walls and the formation of the side wakes affect the side contraction of the nappe (Horton, 1907) and thus the capacity of the TPWs (Pospíšilík et al., 2024). In the case of fully contracted TPWs, there is no change in their capacity with change of approach channel width (Bos, 1989). In the case of partially contracted nappes, the weirs are called partially contracted weirs and in the case of fully contracted nappes, they are called fully contracted weirs (Bos, 1989). The definitional value for their differentiation presented Kulin and Compton (1975) for a notch angle of 90°. Fully contracted weirs have smaller discharge coefficient than partially contracted weirs. The change of discharge coefficient is caused by the change of nappe contractions. Description of discharge coefficient for fully contracted and partially contracted TPWs with a triangular notch and zero height was presented by Pospíšilík et al. (2024). They also determined the boundary between fully and partially contracted weirs based on the change of discharge coefficient. They found that a 1% change of discharge coefficient (discharge) occurs at a dimensionless approach channel width of value 0.25 and 2% change occurs at a value of 0.35.

Flow in an approach channel is influenced by backwater curve caused by TPW and by friction against the channel surface (Clemmens et al., 2001). In the case of small effect of backwater curve and small cross-sectional area of approach channel (high value of approach velocity), the water surface within the recommended section of approach channel for measurement water surface level (two to four times the maximum head) can be affected by waves and by a non-negligible slope (Clemmens et al., 2001). The method of water surface level measurement and location of cross-section for measurement then affects the determination of the head and thus the accuracy of the discharge determination. This effect has not yet been quantified for

partially contracted TPWs with triangular notch and with zero weir height.

The use of partially contracted TPWs with triangular notch is often required in confined space conditions such as drainage channels in dam galleries, small wastewater treatment plants, etc., where TPWs with small triangular notch angles are particularly suitable. Unfortunately, the current characteristics in the case of partially contracted TPWs with small angle of triangular notch are still insufficiently investigated.

Experimental research on the flow over TPWs with triangular notch is very extensive, a detailed summary is given by Pospíšilík and Zachoval (2023). Because of the extensive research, only the most significant researches related to partially contracted weirs are presented here. The basic measurements were published by Thomson (1858; 1861), Barr (1910), Strickland (1910), King (1916), Cone (1916), Yarnall (1912; 1927), Pardoe (Schoder and Turner, 1929), Greve (1930; 1932; 1945), Barrett (1931), Allerton (1932) and Lenz (1942). Extensive research focused mainly on the influence of the approach channel width and the weir height was carried out by Numachi et al. (1940a; 1940b) and Numachi and Hutizawa (1941a; 1941b; 1942a; 1942b). The minimum approach channel length and the use of measurement boxes were dealt with Numachi and Saito (1948; 1951) and Milburn and Burney (1988). The use of TPWs with a triangular notch in confined conditions was studied by Hattab et al. (2019), Pospíšilík (2023), Pospíšilík and Zachoval (2023) and Pospíšilík et al. (2024). All of the above studies have focused primarily on the determination of the discharge coefficient. There is a minimal amount of information about flow characteristics; therefore, this study aims to supplement this lack of data.

Numerical simulations of flow over the weirs have also been addressed by many authors. Most authors focused on broad crested and short crested weirs. Only few authors focused on the TPWs with triangular notch. Abd El-Hady Rady (2011) simulates flow over TPWs using two-dimensional (2D) and three-dimensional (3D) techniques for estimating and validating the discharge coefficient. He used FLOW-3D software (Flow Science, 2024) with the fractional area/volume method (FAVOR) (Mampaey and Xu, 1995) with the renormalization group (RNG) κ-ε turbulence model (Hanjalić and Launder, 1976; Yakhot and Orszag, 1986). He found that the discharge coefficient estimated from simulation is in good agreement with those listed in the literature (±3 % error). Zachoval and Roušar (2015) tested many turbulent models for describing flow characteristics of flow in front of broad crested weir. They found that two-layer Shear Stress Transport (SST) model provides the most reliable results from all used models. Al-Dabbagh and Al-Zubaidy (2018) evaluated flow behaviour over broad-crested weirs with a triangular cross-section under different flow conditions and different angles of cross-section. For simulation of flow was used ANSYS Fluent software with κ-ε turbulence model. Authors determined flow characteristics, water surface level, and pressure acting on the weir. Rezazadeh et al. (2020) used OpenFOAM software (OpenCFD, 2024) with RNG κ-ε turbulence model and volume of fluid (VOF) method (Hirt and Nichols, 1981) to analyse the flow over TPWs with triangular, rectangular, and trapezoidal notch. They compared water surface profile and discharge coefficient determined from numerical simulations and from experimental data. They state a good agreement. Simulation showed that the flow contraction caused by TPWs created local increase of water surface upstream of the weir. Saadatnejadgharahassanlou et al. (2020) simulated 3D flow over a TPWs with multi-segment triangular notches. They used ANSYS Fluent software, VOF method, and a Reynolds stress model (RSM) and three types of the k-ε turbulence models. Results indicated that the RSM exhibited higher accuracy in defining the velocity distribution, complex flow pattern, and predicting the hydraulic jump formation downstream of the weir. Sinclair et al. (2022) studied flow over a TPW with rectangular full-width notch using FLOW-3D software to identify the optimal operating range under which the weir functions with accuracy as a free-flowing measurement device. They compared both velocity and pressure profiles in dimensionless form and discharge coefficient. The research overview indicates that there is a lack of simulations for flow over partially contracted TPWs with a triangular notch. Additionally, it highlights, that researchers have paid less attention to the characteristics of the computational mesh, which is crucial for obtaining credible simulations. Therefore, this study provides new recommendations for simulating flow over partially contracted TPWs with a triangular notch.

A review of experimental investigations and numerical simulations show that for flow over partially contracted TPWs with triangular notch, there is currently no detailed information about the flow characteristics, no recommendations for the construction of a numerical model and no defined boundary between partially contracted weirs and fully contracted weirs based on the flow characteristics. Therefore, this paper deals with their determination for the case of a TPWs with a triangular notch with angle of 20.23° and with zero weir height above the approach channel bottom. The selected angle of notch was chosen due to the ability to measure small discharges in very confined space conditions with relatively high accuracy (Shen, 1981). This is the smallest notch angle (20°) recommended by the standard ISO (ISO, 2017) for measurement of discharge. The zero weir height was also chosen due to its use in very confined space conditions.

2 MATERIALS AND METHODS

The origin of the coordinate system used to describe the flow was given by the vertex of the notch. Vertical against the direction of the acceleration due to gravity g was the axis z, longitudinally in the direction of the flow was the axis x and transversely was the axis y. TPW with triangular notch (Figure 1) was described by the notch angle α and by the triangular notch vertex elevation – weir crest level Z_P. Approach channel with a rectangular cross-section and zero bottom slope were described by the approach channel width B. Overflow was described by the water surface level $Z_{h,U}$ measured at an agreed upstream distance from the thin-plate weir ($-2 \cdot h_{U,max}$ to $-4 \cdot h_{U,max}$, where $h_{U,max}$ is the maximum head (ISO, 2017)). For the sake of clarity, the distance $x_U = -2 \cdot h_{U,max}$ was chosen. Head was $h_U = Z_{h,U} - Z_P$ and height relative to the notch vertex was $h = Z_h - Z_P$. The dimensionless distance $x^* = x/h_U$ and dimensionless height $h^* = h/h_U$ were defined relative to the head. The notch width at the measured level of water surface for determine head was $b_{TPW} = 2 \cdot h_U \cdot \tan(\alpha/2)$. The dimensionless nappe width $b^* = b/b_{TPW}$ and the dimensionless distance $x_b^* = x/b_{TPW}$ were defined relative to the notch width. For graphical representation and clarity, the dimensionless approach channel width was used $B_U^* = 1/b_U^* = b_{TPW}/B$. The properties of water were described by density ρ and kinematic viscosity υ, properties of air surrounding the nappe by density ρ_a and kinematic viscosity υ_a. The interface forces between water and air were described by surface tension σ.

Since no suitable experimental data was available, it was necessary to conduct experimental research. The measurements

were carried out on the equipment described by Gabriel (2023). A TPW with a triangular notch of angle $\alpha = 20.23°$ was used.

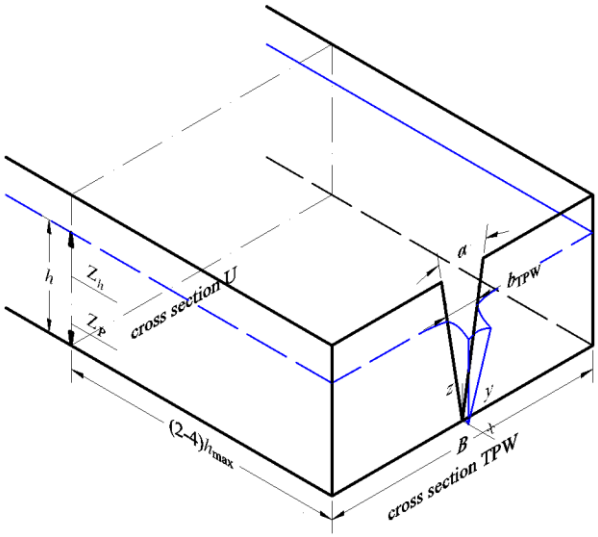

Fig. 1. Diagram of marking of variables.

The water surface level Z_h was measured in the longitudinal plane of symmetry $y = 0.000$ m at the discharge given by the head $h_U = 0.180$ m and at different widths of the approach channel $B = 0.064$ m, 0.100 m, 0.200 m, 0.300 m, 0.500 m. The smallest value of B corresponds to the width of the notch b_{TPW} for given h_U and larger values of B could not be made due to the limitations of the experimental equipment. In cross-section U in the approach channel at distances of x_U, the Froude number was determined as $Fr_U = Q/(B \cdot g^{1/2} \cdot h_U^{3/2})$ and Reynolds number $Re_U = Q/(B \cdot \upsilon)$, where Q is discharge. Their values were in the ranges $0.030 \leq Fr_U \leq 0.286$ and $7156 \leq Re_U \leq 67526$, thus, it was always a turbulent flow in the subcritical regime, which meets the condition $Fr_U < 0.5$ (Clemmens et al., 2001) to provide suitable conditions for relatively accurate measurements of water surface level. Water surface level were measured at 10 distances x presented in Table 1 and showed in Figure 3. A digital point gauge with resolution 0.01 mm was used. The time-mean value of Z_h (Table 1) was taken for the evaluation (acceptable pulsation to ±0.1 mm during 180 s). The discharges were measured by electromagnetic flow meter DN50. The free-falling nappe was not aerated in the measurement range.

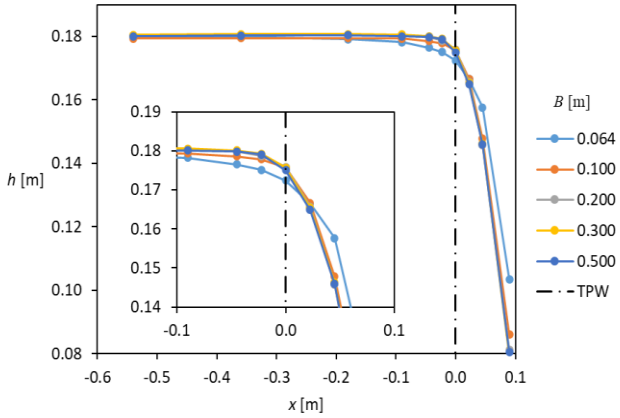

Fig 2. Measured water surface profiles in longitudinal section.

The velocity field was measured only for the case $B = 0.500$ m and $h_U = 0.180$ m (Figure 3). Measured were the horizontal velocity components $v_{x,y}$ in horizontal plane $z = 0.150$ m (black in 0), the longitudinal velocity components v_x in vertical plane $y = 0.000$ m (plane of longitudinal symmetry, orange in Figure 3) and the longitudinal velocity components v_x in transverse plane $x = -0.360$ m (cross-section U, green in Figure 3). An UVP-DUO (Met-Flow SA, 2020) device was used to measure with one 4MHz probe with internal diameter of active element 5 mm. The measurement time for the one velocity component value at the measured point was 120 s. The measured points were chosen in an orthogonal arrangement (grid) at a mutual distance 0.020 m. The reliability of the measured velocity values in the longitudinal direction was carried out by comparing the discharge Q determined by an electromagnetic flow meter with value 0.00366 m^3/s and determined from the velocity field and flow area with value 0.00367 m^3/s (error 0.3 %).

Table 1. Values of Z_h (m).

B (m)		**0.064**	**0.100**	**0.200**	**0.300**	**0.500**
Q (l/s)		**4.382**	**3.825**	**3.644**	**3.620**	**3.727**
x (m)	0.090	0.1035	0.0860	0.0812	0.0796	0.0805
	0.045	0.1576	0.1478	0.1459	0.1463	0.1459
	0.023	0.1665	0.1667	0.1657	0.1654	0.1649
	0.000	0.1724	0.1757	0.1759	0.1757	0.1750
	−0.023	0.1751	0.1779	0.1787	0.1793	0.1791
	−0.045	0.1765	0.1786	0.1799	0.1801	0.1798
	−0.090	0.1783	0.1794	0.1803	0.1806	0.1801
	−0.180	0.1791	0.1795	0.1804	0.1808	0.1804
	−0.360	0.1800	0.1795	0.1804	0.1807	0.1803
	−0.540	0.1800	0.1794	0.1803	0.1805	0.1801

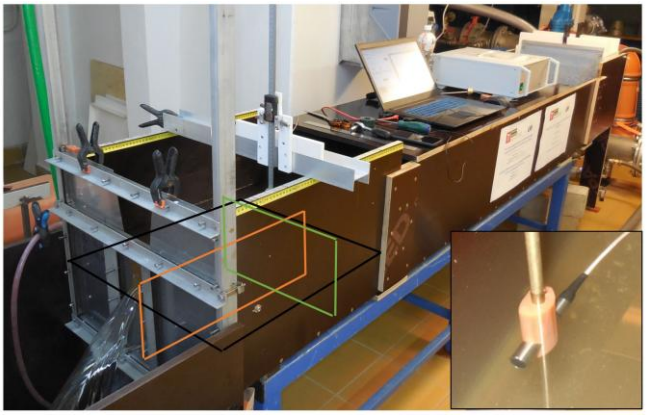

Fig. 3. View of the flume during a velocity field measurement, probe in detail, scheme of planes for measurement.

The kinetic energy correction factor at the cross-section U was $\alpha_{v,U} = 1.078$. It was calculated from the equation $\alpha_{v,U} = \int(v_U^3 \cdot dA_U)/(\bar{v}_U^3 \cdot A_U)$, where $A_U = B \cdot h_U$, v_U is the point velocity and $\bar{v}_U$ is the cross-sectional velocity (Streeter, 1942). The achieved value corresponds to the values (1.03–1.10) achieved in approach channels with the same cross-section (Bos, 1989).

For simulation of flow over TPW with triangular notch the ANSYS Release 2023 R2 software and Ansys CFX module was used (ANSYS, 2024a). The full buoyancy model was used (Van Maele and Merci, 2006) that involves multiphase flow (water, air). For the isothermal interpenetrating multiphase homogeneous coupled model, the Euler-Euler approach and VOF method was used. The continuity and momentum Reynolds-averaged Navier-Stokes (RANS) equations for both fluids were used. System of equations was closed by shear stress transport (SST) κ-ω turbulence model (Menter, 1993; Menter, 1994) in accordance with the recommendation of Zachoval and Roušar (2015) and Menter et al. (2021). SST turbulence model effectively blend the κ-ω model in the near-wall region (inner layer) with κ-ε model in the far region (outer layer). For interpretation of the surface tension as a continuous volume force in the direct vicinity of the interface, the continuum surface force (CSF) model has been implemented (Brackbill et al., 1992).

Creating a numerical model for simulating clean water flow through an approach channel of rectangular cross-section and free flow over a TPW with a triangular notch of angle 20.23° involved creating the geometry of the computational domain, constructing the mesh, determining the material properties of the fluids, specifying the initial and boundary conditions (Inlet, Opening, Symmetry, and Wall), and setting up the calculation method.

Table 2. Geometry of Bodies.

ID	Shape	Dimensions (length, width, height)
Body_1	rectangular cuboid	0.810 m, B/2, 0.200 m
Body_2	rectangular cuboid	0.009 m,B/2 – 0.050 m, 0.200 m
Body_3	rectangular cuboid with wedge cut out which represent triangular notch of TPW	0.020 m, 0.050 m, 0.200 m
Body_4	rectangular cuboid	0.190 m, 0.075 m, 0.200 m

Corresponding to 5 selected approach channel widths B, 5 separate geometric models were created. Geometric models included the volume of approach channel – Body_1 and Body_2, volume around triangular notch – Body_3 and outflow volume – Body_4 (Figure 4). Because of the assumption of symmetrical flow according to the longitudinal plane of symmetry $y = 0.000$ m crossing the notch vertex of the TPW, the geometric models represented only half of the real flow, which reduced considerable computing time. Division of the geometric model into individual Bodies made it possible to use meshes with different types and densities, which in the case of flow with variable character was beneficial (accuracy and computational time). The geometry of Bodies is described in Table 2.

A computational mesh was created for each geometric model. Due to the continuity and connectivity of the Body meshes and the geometric constraints caused by the triangular notch, two basic types of meshes with corresponding elements were used. Meshes of Body 1, 2 and 4 were structured with hexagonal elements. The use of hexagons was deliberately chosen because of the orthogonal shapes of the volumes, minimization of computational time and the unambiguity of data evaluation in the chosen planes. For Body 3, an unstructured mesh with tetrahedrons was used. The use of tetrahedrons allowed to reduce the size of the elements in the triangular notch region of the TPW and to respect the shape constraints of the elements.

For the case $h_U = 0.180$ m and $B = 0.100$ m an analysis of the influence of element sizes of the Body 1, 2 and 4 (l_1, l_2, l_4) and element size of the Body 3 (l_3, including the value of the minimum element size when using the proximity method $l_{3,min}$) on water surface level was provided. The evaluation of the influence was carried out by comparison of the simulated head $h_{U,sim}$ and measured head h_U. The value $h_{U,sim}$ was determined from the pressure p at the bottom of the approach channel in cross-section U $h_{U,sim} = p/(\rho \cdot g)$. The accuracy of the overflow head calculation was characterised by the relative error $\delta h_{U,sim} = 100 \cdot (h_{U,sim} - h_U)/h_U$ (%). The total number of meshes used for the analysis was 10. The values of element sizes and relative errors are given by Table 3 and graph in Figure 5. Table 3 and Figure 5 show that the relative error decreases with decreases element size. The main influence on the reduction of the error was the setting of the element size Body 3 corresponding to plate thickness of the TPW l_{TPW}, which was $l_{TPW} = 0.001$ m (the smallest value of the recommended values from (ISO, 2017)), as well as the use of the proximity method. A similar correlation, but multiple, was found in the case of Body 1, 2 and 4. For this reason, the mesh size for further description was expressed relative to the plate thickness TPW, thus $l_i^* = l_i/l_{TPW}$, where $i = 1, 2, 3, 3,\text{min}, 4$. The values were added to Table 3. The analysis showed that the relative error did not decrease further when the elements were reduced below a certain threshold (mesh ID 8, 9, 10). For this reason, a mesh that can be characterized by the relative lengths of the elements $l_1^* = l_2^* = l_4^* = 2.0$, $l_3^* = 0.7$, and $l_{3,min}^* = 0.2$ was used for further calculations (green highlight in Figure 5). For individual approach channel widths B according to the recommendations of the above analysis, meshes were created with the numbers of elements indicated by Table 4. An example of the used mesh for $B = 0.200$ m is shown in the Figure 6. The Grid-Convergence Index (GCI) (Roache, 1994) was also used to evaluate the density of mesh with ID 8. The analysed quantity was h_U, depending on the element size l_3 in Body_3. Meshes with IDs 3, 7, and 8 were used for the analysis. The resulting GCI values were $GCI_{3,7} = 0.31$ % and $GCI_{7,8} = 0.14$ %, indicating that the mesh is sufficiently dense.

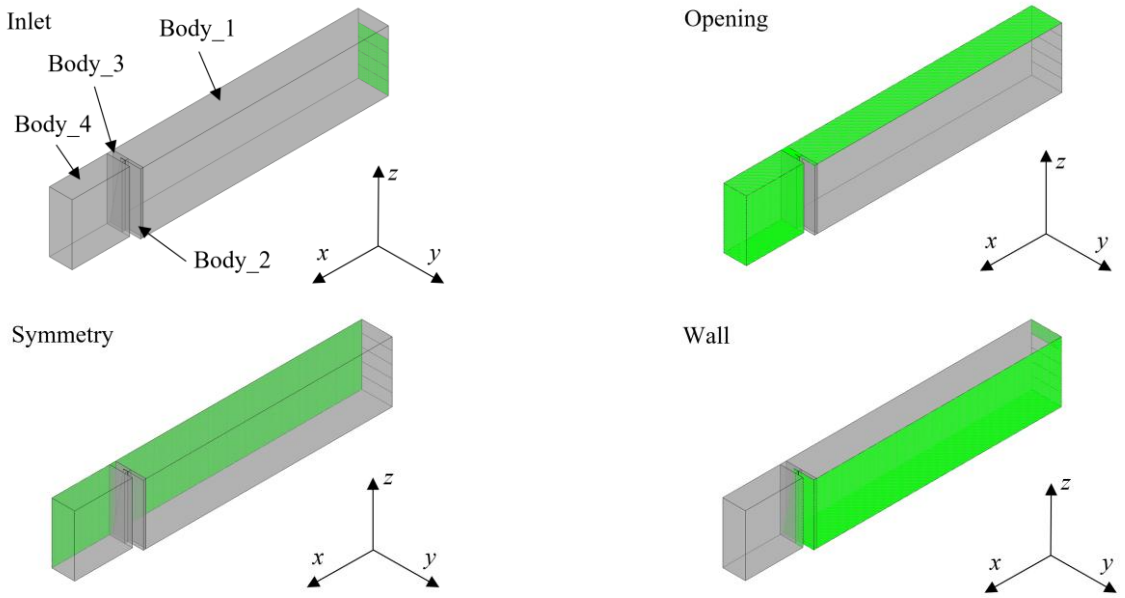

Fig. 4. Definition of Bodies and locations of the faces with types of boundary conditions.

Table 3. Overview of the used mesh.

Mesh ID	Body 1, 2, 4		Body 3				$\delta h_{U,sim}$	
	l_1, l_2, l_4 (m)	l_1^*, l_2^*, l_4^*	l_3 (m)	$l_{3,min}$ (m)	l_3^*	$l_{3,min}^*$	(m)	(%)
1	0.010	10	0.0100	–	10.0		−0.0147	−8.2
2	0.008	8	0.0080	–	8.0		−0.0119	−6.6
3	0.004	4	0.0040	–	4.0		−0.0066	−3.7
4	0.004	4	0.0010	0.0005	1.0	0.5	−0.0021	−1.2
5	0.003	3	0.0010	0.0005	1.0	0.5	−0.0019	−1.1
6	0.003	3	0.0005	0.0002	0.5	0.2	−0.0017	−1.0
7	0.002	2	0.0010	0.0005	1.0	0.5	−0.0012	−0.6
8	0.002	2	0.0007	0.0002	0.7	0.2	−0.0007	−0.4
9	0.002	2	0.0006	0.0002	0.6	0.2	−0.0007	−0.4
10	0.001	1	0.0007	0.0002	0.7	0.2	−0.0007	−0.4

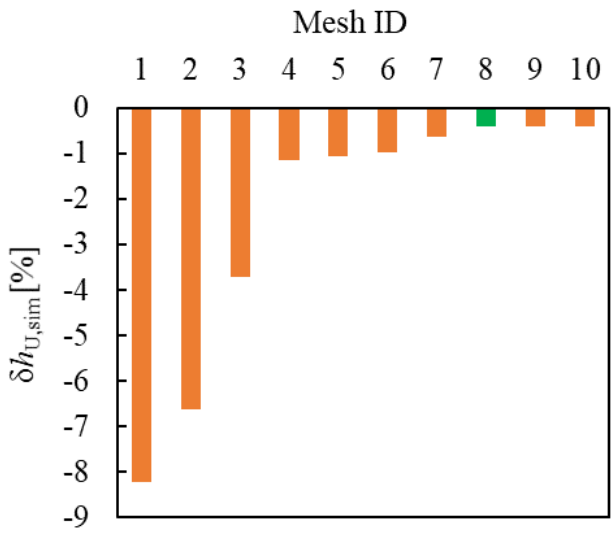

Fig. 5. Influence of mesh ID on $\delta h_{U,sim}$.

Table 4. Characteristics of geometric model meshes based on the approach channel widths.

B (m)	Number of Elements
0.500	9 791 366
0.300	7 740 383
0.200	6 717 269
0.100	5 737 851
0.064	4 187 146

The flow of two fluids was simulated: water with a density of ρ = 997 kg/m^3 and kinematic viscosity υ = 0.000 000 893 m^2/s and air with a density of ρ_a = 1.185 kg/m^3 and viscosity υ = 0.000 0155 m^2/s at reference pressure 101 325 Pa (White, 2011). Water was used as the main fluid with surface tension σ = 0.072 N/m (White, 2011). The effect of gravitational acceleration was specified g = 9.806 65 m/s^2 against the direction of the axis *z*.

The initialization condition was a fully flooded geometric model with hydrostatic pressure distribution.

Surfaces with boundary conditions (Inlet, Opening, Symmetry, Wall) are shown in Figure 4. For the flow simulations at different heads, four surfaces were uniformly defined Inlet_04

in the range of 0.000 m ≤ z ≤ 0.040 m, Inlet_08 in the range of 0.040 m ≤ z ≤ 0.080 m, Inlet_12 in the range of 0.080 m ≤ z ≤ 0.120 and Inlet_16 in the range of 0.120 m ≤ z ≤ 0.160 m. The use of four surfaces allowed the setting of a stable water inflow at different heads without significantly affecting the flow in the cross-section U. For h_U = 0.06 m and 0.08 m the Inlet_04 was used; for h_U = 0.10 m and 0.12 m Inlet_04 and Inlet_08 were used; for h_U = 0.14 m and 0.16 m Inlet_04, Inlet_08 and Inlet_12 were used; and for h_U = 0.18 m all Inlets were used. The water inflow specified by the cross-sectional velocity was set perpendicular to the Inlet surfaces with a turbulence intensity of 5%. The cross-sectional velocity values for each heads h_U were determined by calculation from experimental research published by Pospíšilík and Zachoval (2023) and Gabriel (2023). The inflow of air to the model has not been adjusted. Relative pressure 0 Pa was set on the Opening surfaces. On the Symmetry surfaces the balance of forces acting in the symmetry plane was ensured. A hydraulically smooth surfaces were assumed on the Wall surfaces.

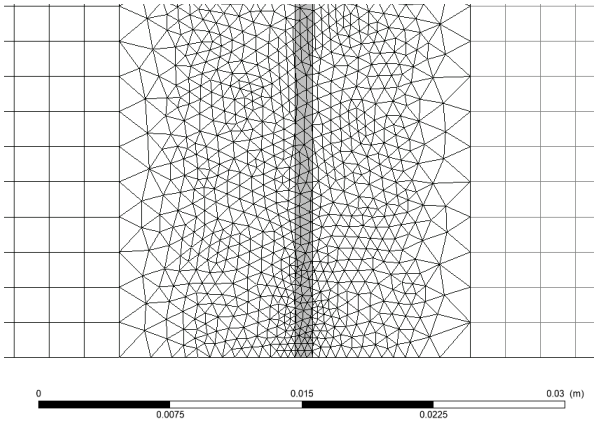

Fig. 6. Example of the mesh with ID 8 in the plane of symmetry around the notch vertex for B = 0.200 m (grey area is TPW).

Solver was set to advection scheme with high resolution and fluid timescale was set constant 0.05 s. The convergence criterion was a change in the water surface level over time less than $1 \cdot 10^{-6}$ m in the cross-section U. All calculations were stable and for water was always achieved RMS mass < $3 \cdot 10^{-5}$.

For each model geometry of widths B presented in Table 4, the flow simulations were carried out at h_U = 0.060 m, 0.080 m, 0.100 m, 0.120 m, 0.140 m, 0.160 m, 0.180 m. Thus, a total of 35 simulations were performed.

3 VALIDITY OF SIMULATIONS

The validity of the simulated flow characteristics was evaluated by comparing the data from the simulations with data from experimental research. The velocity fields, heads, and water surface levels were compared.

A comparison of velocity fields determined by simulations and by measurements was made for the case of B = 0.500 m and h_U = 0.180 m. The Figure 7 a) shows the field of the simulated horizontal velocity components $v_{x,y}$ (thin lines of isolines) together with the field of measured velocity components (thick lines of isolines) in the z = 0.150 m plane, which is supplemented by velocity vectors and by positions of measurement points. The Figure 7b) shows field of simulated longitudinal velocity components v_x together with measured in the vertical plane y = 0.000 m (plane of longitudinal symmetry). The Figure 7c) shows field of simulated longitudinal velocity components v_x together with measured in the transverse plane x = −0.360 m. It is clear from the figures that the velocity fields near the TPW are relatively similar. Noticeable differences are only near the water surface (violet line in the figures), where the effect of the Inlet boundary condition in the numerical simulations is propagated. This is particularly noticeable in the transverse profile x = −0.360 m. It should be noted that numerical simulations were performed in case of the short approach channel, which describes Pospíšilík and Zachoval (2023), and the measurements were made in a long approach channel, which describes Gabriel (2023), so these differences were to be expected. From the measured velocity vectors and numerical simulations velocity fields, it is evident that a wakes forms in the corner of the side wall of the approach channel and the TPW wall. The size of wakes is decreasing when increasing the B_U^*. Wake at B_U^* = 1 does not occur on the water surface.

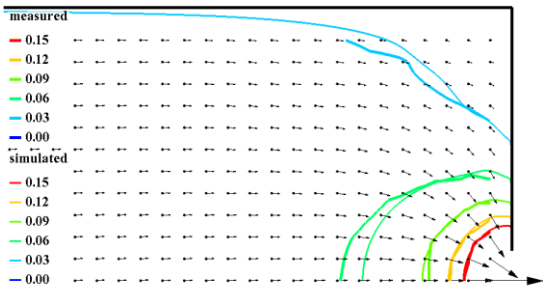

a) Horizontal velocity components $v_{x,y}$ in plane z = 0.150 m (h^* = 0.833).

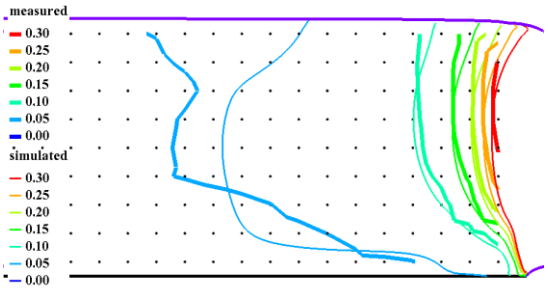

b) Longitudinal velocity components v_x in the vertical plane y = 0.000 m.

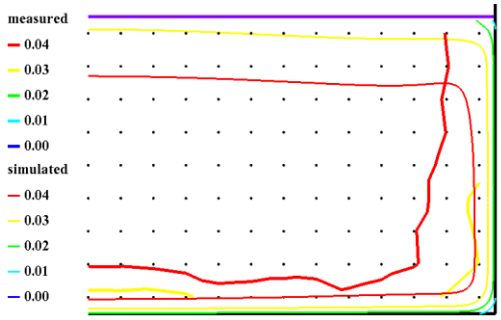

c) Longitudinal velocity components v_x in transverse plane x = −0.360 m (x^* = −2.000).

Fig. 7. Comparison of velocity fields for h_U = 0.18 m.

For the comparison of heads, the values determined by Pospíšilík (2023) and Gabriel (2023) were taken for all values of B. The relative error $\delta h_{U,sim}$ of the simulated head was used for the assessment. In Figure 8 the relative error of the simulated head $\delta h_{U,sim}$ is shown depending on the measured head h_U for individual approach channel widths B. From Figure 8 it is evident that the value $\delta h_{U,sim}$ does not exceed the relative error ±2% in full range of h_U. This is consistent with the uncertainties

of the experimental measurement of Pospíšilík (2023). For the values of h_U = 0.06 m there is an increase in $\delta h_{U,sim}$ compared to other h_U values. This may be due to the combined effect of viscosity and surface tension, of which effect increases with decreasing head (Pospíšilík and Zachoval, 2023). The values of $\delta h_{U,sim}$ for the approach channel width B = 0.064 m are larger compared to the others. This may be due to incorrectly estimated roughness of the wall surfaces (waterproof plywood walls – hydraulically smooth surface), or due to the effect of surface tension, but also due to the relative error in determining the width of the approach channel during the measurement.

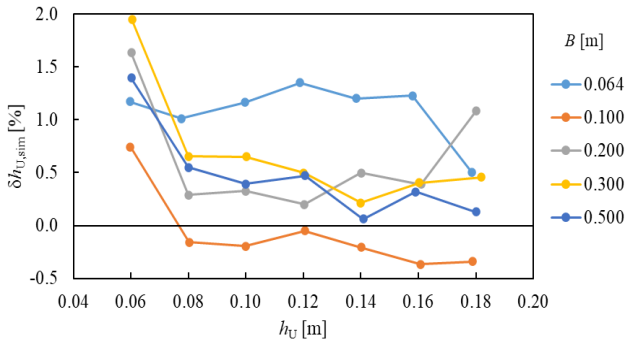

Fig. 8. Relative simulated head error $\delta h_{U,sim}$ depending on the measured head h_U for individual approach channel widths B.

The measured water surface levels were used to compare the simulated water surface levels. The evaluation is made in Figure 9 by graphical dependence of the dimensionless head h^* on the dimensionless distance x^* for each B_U^*. In Figure 9 the continuous lines represent the simulated values and points measured. A plot of the detail of the area around the TPW is embedded in the graph for better readability. Comparison of the water surface levels shows that the levels are simulated relatively accurately over the entire range of values B_U^*. For example, the relative error of the dimensionless height in the TPW profile (x^* = 0, dashed line in Figure 9) $\delta h_{TPW,sim}^*$ is up to ±0.5 %. Relative error value δh_{sim}^* is for the values of $x^* < 0$ practically the same, but for values $x^* > 0$ increases with increasing value of x^*.

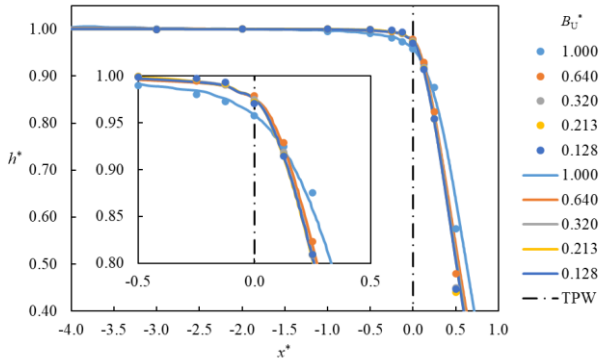

Fig. 9. Dimensionless height h^* dependency on dimensionless distance x^* for each B_U^*, points – measurements, lines – simulations.

The above comparison overview shows that the simulation is relatively accurate.

4 RESULTS

Due to the extent of the numerical simulations performed and the relative similarity of the flow characteristics, only one detailed example result for a geometric model with a width of B = 0.200 m is presented. This example corresponds to the boundary between a fully contracted and partially contracted weir. All results were presented by Pospíšilík (2023). In Figure 10 is a view on the overflow at h_U = 0.180 m. Figure 10 shows the surface velocity of water v. It can be seen that the surface velocities increase mainly against the direction of the z axis. It is evident from the above that the surface velocities depend in the nappe mainly on the gravitational acceleration. Figure 11 shows the velocity fields in the plane of symmetry y = 0.000 m at all overflow heads h_U. The figure shows that the water velocity v increases as the overflow head increases. It can also be seen here that in the approach channel the velocity increases in the forward direction of the axis x, whereas in the free nappe it increases mainly against the direction of the axis z. Figure 12 shows the velocity fields in horizontal planes at h_U = 0.180 m. Figure 11 together with Figure 12 show that the maximum flow velocity in the TPW cross-section is reached near the vertex of the triangular notch. The downstream change in the shape of the free nappe is then due to the velocity field at the cross-section TPW. The upper part of the flow at the cross-section TPW (near the surface) has a small value of specific kinetic energy and the direction of the velocity vectors is inclined downwards. In contrast, the lower part of the flow (near the vertex of the triangular notch) has a large value of specific kinetic energy and the direction of the velocity vectors is sloped slightly upwards. This causes that the lower part of the nappe supports the upper part of the flow, and under the action of acceleration due to gravity, the free nappe then expands laterally (Figure 12).

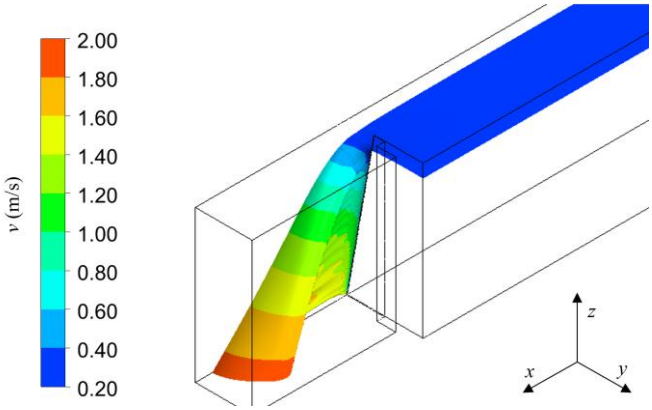

Fig. 10. Surface velocities v for head h_U = 0.18 m.

Due to the applicability of contracted TPWs with a triangular notch of angle 20.23° and a zero weir height for flow measurement, the recommended range for measurement of the water surface level was verified and the boundary between the fully contracted weir and the partially contracted weir was determined.

The effect of approach channel friction on the water surface slope within the recommended range for its measurement, i.e. $-4 \le x^* \le -2$, was determined from the simulated values at the head h_U = 0.18 m. Relative difference in dimensionless heights δh_{sim}^* within a recommended range x^* increases with increasing value B_U^*. Throughout the recommended range of x^*, the values are up to 0.6 %. The effect of friction is, therefore, relatively small.

Determination the boundary separating the fully contracted weir and the partially contracted weir and description of the flow characteristics were performed only for the maximum head $h_{U,max}$ = 0.18 m due to the scope of the simulations.

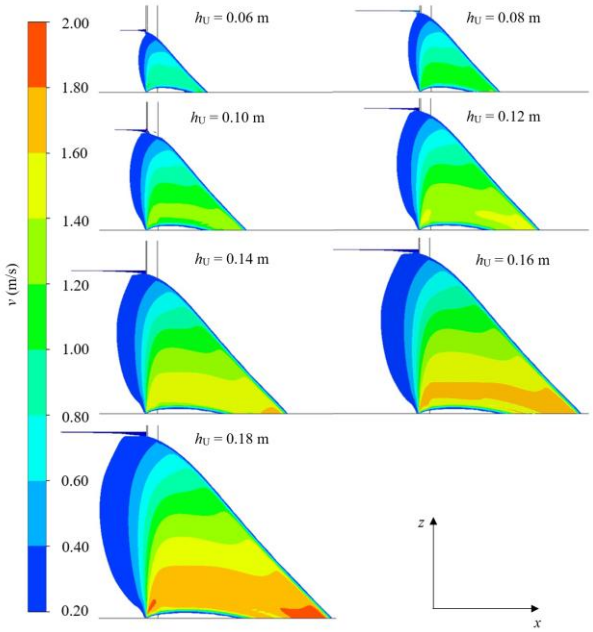

Fig. 11. Velocities v in plane symmetry $y = 0.000$ m for different heads h_U.

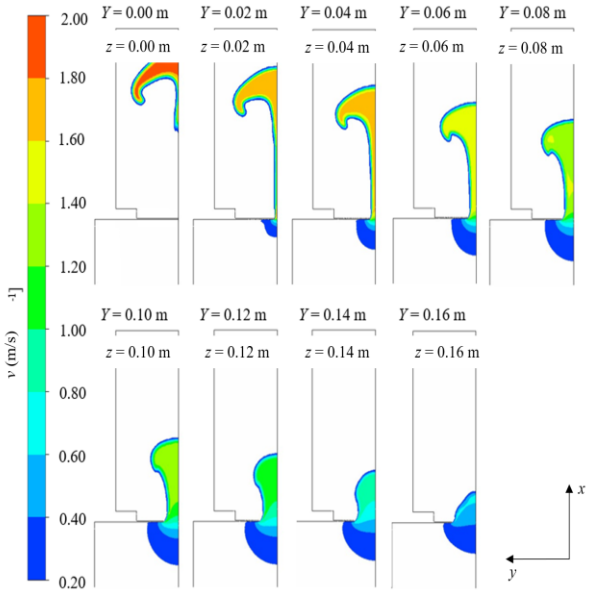

Fig. 12. Velocities v in horizontal planes z for $h_U = 0.18$ m.

The description of the flow characteristics was focused on the effect of changing the approach channel width on the change of the nappe width in the vertical and horizontal planes. For description of horizontal changes of nappe width, the results from numerical simulations were used. The chosen plane was $z = 0.120$ m, thus $h^* = 2/3$, because there is a significant downstream contraction of the nappe (compared to the lower levels) and at the same time the contraction is not affected by the nappe widening to the sides in its upper part. Figure 13 shows the merged water surface positions.

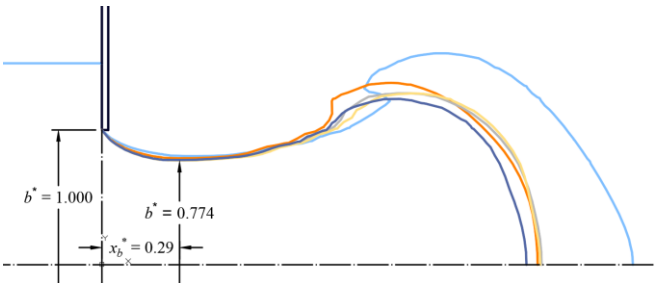

Fig. 13. Nappe in level $z = 0.120$ m at $h_U = 0.18$ m.

The influence is evaluated in plane $x_b^* = 0.29$, where the largest side contraction of the nappe occurs in a case of fully contracted weir. The effect of changing the nappe width at a given plane is demonstrated in Figure 14 by dependence ratio b^*/b_0^* on B_U^*, where b_0^* is the dimensionless nappe width in the case of a fully contracted weir. For description of vertical changes of the nappe, the results from experimental research were used. The plane of symmetry and the transverse profile $x^* = 0.25$ were selected. The effect of the change of the upper nappe envelope in a given profile is demonstrated in Figure 14 by dependency of ratio h^*/h_0^* on B_U^*, where h_0^* is the dimensionless height of the upper nappe envelope in the case of a fully contracted weir. In the case of both the above-mentioned dependencies of ratios, it can be seen that boundary between the fully contracted weir and the partially contracted weir was the same and that the $B_U^* = 0.32$. In summary, within the range of $0.00 \le B_U^* \le 0.32$, the shape of the nappe envelope remains practically unchanged in both the longitudinal plane of symmetry and the horizontal plane at $h^* = 2/3$. This corresponds to the area of fully contracted weirs. However, in the range of $0.32 < B_U^* \le 1.00$, the shape of the nappe envelope changes, which corresponds to the area of partially contracted weirs. Within this given range of B_U^*, the values of b^*/b_0^* and h^*/h_0^* increase with the increasing B_U^*.

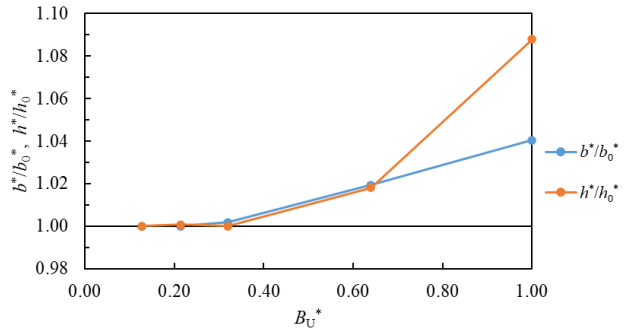

Fig. 14. Change of nondimensional nappe width b^* expressed by the ratio b^*/b_0^* in plane $x_b^* = 0.29$ and change in dimensionless height h^* expressed by the ratio h^*/h_0^* in plane $x^* = 0.25$ caused by a change of the nondimensional approach channel width B_U^*.

5 DISCUSSION

A description of the flow characteristics was made for a free overflow of clean water for a partially contracted TPW with a triangular notch of angle 20.23° and a zero weir height above the approach channel bottom of rectangular cross-section at approach channel widths in range $0.064 \text{ m} \le B \le 0.500$ m and heads in range $0.060 \text{ m} \le h_U \le 0.180$ m, i.e. the full range of the partially contracted weir at relatively small heads (here detailed presented only for $h_U = 0.180$ m). It is probable that the flow characteristics at different heads will be influenced by the scale

effect in the same manner as the discharge (Pospíšilík et al., 2024). The TPWs with different notch angles may have a different value of nondimensional approach channel width for the boundary between fully and partially contracted weirs. Different weir heights will change the flow characteristics in front of the TPWs, the flow will be more affected by vertical velocities. For the reasons mentioned above, the findings cannot be extrapolated.

Experimental research and numerical simulations were performed to describe the flow characteristics. The numerical simulations described the flow characteristics in regions of flow where measurements were difficult to make or with a large degree of uncertainty of determination (especially the velocity fields near the walls and in the nappe). Given that the SST turbulence model yields relatively reliable results near the walls and in the wakes (Menter et al., 2021) it is unlikely that the flow pattern at a distance of up to 0.02 m from the wall would be fundamentally different. However, the velocity field in the free overflow section remains unverified.

The experimental research allowed to quantify the validity of the numerical simulations. The relative errors of the head results determined by the simulations Figure 8 corresponded to the uncertainty of the determination of the measurements (relative error ±2 %). From this, it can be concluded that the simulations have a very good accuracy.

The results from the experimental research and numerical simulations were converted into dimensionless forms for further analysis and generalisation. Based on these, it was possible to evaluate the changes in dimensionless position of the upper part of the nappe in the longitudinal plane of symmetry and the changes in dimensionless nappe width in the selected vertical plane both induced by the change of dimensionless approach channel width. The dimensionless expression will enable comparison with other experimental data in the future.

6 CONCLUSION

The main result of the analyses performed was the determination of the boundary between partially contracted and fully contracted weir based on nappe characteristics. This boundary was determined by the dimensionless width of the approach channel $B_U^* = 0.32$. This value corresponds with the values determined by the change of discharge (coefficient of the relative width of the approach channel) presented by Pospíšilík et al. (2024) for the same case of weir. They found 1 % change in discharge for $B_U^* = 0.25$ and 2 % change for $B_U^* = 0.35$.

An important observation is that the influence of the longitudinal water surface slope in the section recommended for water surface level measurement ($-4 \leq x^* \leq -2$) is negligible (relative difference of dimensionless height is < 0.6%), thus it can be neglected for practical use and measurements can be made in any cross-section in the recommended section of approach channel.

The results showed that even when the width of the approach channel is the same as the width of the triangular notch at the measured level, lateral contractions occur, and sufficient rise of the water surface level occurs in the approach channel. Therefore, a TPW with a triangular notch of angle 20.23° and zero weir height above the bottom of the approach channel of rectangular cross-section is suitable for discharge measurement over the full range of the partially contracted weirs. This knowledge expands the application possibilities for measuring small discharges in confined space conditions.

Acknowledgements. The article was created with the support of the project FAST-S-23-8233 “Sensitivity analysis of selected input parameters of numerical models in hydraulic calculations of water flow”.

Nomenclature

A_U	area of cross-section U (m^2)
b	nappe width (m)
b^*	nondimensional nappe width
b_0^*	nondimensional nappe width in case of fully contracted weir
b_{TPW}	notch width in the measured level (m)
B	approach channel width (m)
B_U^*	nondimensional approach channel width
Fr_U	Froude number at cross-section U
g	standard acceleration due to gravity (m/s^2)
h	height relative to notch vertex (m)
h^*	nondimensional height
h_0^*	nondimensional height in case of fully contracted weir
h_U	head, height in cross-section U (m)
$h_{U,max}$	maximum head (m)
$h_{U,sim}$	simulated head (m)
l	element edge length (m)
l_{TPW}	weir crest length in direction of flow (m)
l^*	nondimensional element edge length
p	pressure (Pa)
Q	discharge (m^3/s)
Re_U	Reynolds number at cross-section U
v	point velocity (m/s)
v_U	point velocity at cross-section U (m/s)
$\overline{v}_U$	average velocity at cross-section U (m/s)
v_x	x component of velocity (m/s)
v_{xy}	xy component of velocity (m/s)
x	coordinate (m)
x^*	nondimensional distance
x_b^*	nondimensional distance (relative to b_{TPW})
y	coordinate (m)
z	coordinate (m)
Z_h	water surface level (m)
$Z_{h,U}$	water surface level in upstream distance $2 \cdot h_{U,max}$ (m)
Z_P	weir crest level (m)
α	notch angle (°)
$\alpha_{v,U}$	kinetic energy correction factor at cross-section U
ρ	water density (kg/m^3)
ρ_a	air density (kg/m^3)
υ	water kinematic viscosity (m^2/s)
υ_a	air kinematic viscosity (m^2/s)
σ	surface tension (N/m)
$\delta h_{U,sim}$	relative error of simulated head
δh_{sim}^*	relative error of simulated nondimensional height
$\delta h_{TPW,sim}^*$	relative error of simulated nondimensional height at cross-section TPW.

REFERENCES

Abd El-Hady Rady, R.M., 2011. 2D-3D Modeling of flow over sharp-crested weirs. Journal of Applied Sciences Research, 7, 12, 2495-2505.

Al-Dabbagh, M.A., Al-Zubaidy, S.D., 2018. Evaluation of flow behavior over broad-crested weirs of a triangular cross-section using CFD techniques. The Eurasia Proceedings of Science, Technology, Engineering & Mathematics (EPSTEM), 2, 361-367.

Allerton, R.W., 1932. Flow of water over triangular weirs. Thesis. Princeton University, Princeton.

ANSYS, 2024a. Ansys CFX [software]. https://www.ansys.com/products/fluids/ansys-cfx

ANSYS, 2024b. Ansys Fluent [software]. https://www.ansys.com/products/fluids/ansys-fluent

Barr, J., 1910. Experiments upon the flow of water over triangular notches. Engineering, 89, 435–437, 470–473.

Barrett, F.B., 1931. The flow of water over triangular weirs. Thesis. Princeton University, Princeton.

Bos, M.G., 1989. Discharge measurement structures. 3. ILRI, Deltares. https://repository.tudelft.nl/islandora/object/uuid:bed11d85-f4af-46d1-ba58-7d71f8c8f9c2?collection=research

Brackbill, J.U., Kothe, D.B., Zemach, C., 1992. A continuum method for modeling surface tension, Journal of Computational Physics, 100, 2, 335-354. https://doi.org/10.1016/0021-9991(92)90240-Y

Clemmens, A.J., Wahl, T.L., Bos, M.G., Replogle, J.A., 2001. Water measurement with flumes and weirs. ILRI.

Cone, V.M., 1916. Flow through weir notches with thin edges and full contractions. J. Agric. Res., 5, 23, 1051–1113.

Flow Science, 2024. FLOW-3D [software]. https://www.flow3d.com/

Gabriel, P., 2023. Influence of approach channel width on flow over thin-plate weir with triangular notch. Batchelor Thesis. Brno University of Technology, Brno. (In Czech.)

Greve, F.W., 1930. Calibration of 16 triangular weirs at Prude. Eng. News-Rec., 105, 5, 166–167.

Greve, F.W., 1932. Flow of water through circular, parabolic, and triangular vertical notch-weirs. Eng. Bulletin Purdue University, 40, 2–84.

Greve, F.W., 1945. Flow of liquids through vertical circular orifices and triangular weirs. Eng. Bull. Purdue University, 29, 3, 1–68.

Hager, W.H., 2010. Wastewater Hydraulics. 2. Springer, Heidelberg.

Hanjalić, K., Launder, B.E., 1976. Contribution towards a Reynolds-stress closure for low-Reynolds-number turbulence. J. Fluid Mech. 74, 4, 593–610. https://doi.org/10.1017/S0022112076001961

Hattab, M.H., Mijic, A.M., Vernon, D., 2019. Optimised triangular weir design for assessing the full-scale performance of green infrastructure. Water, 4, 11, 773–790. https://doi.org/10.3390/w11040773

Hirt, C.W., Nichols, B.D., 1981. Volume of fluid (VOF) method for the dynamics of free boundaries. Journal of computational physics, 39, 201–225. https://doi.org/10.1016/0021-9991(81)90145-5

Horton, R.E., 1907. Weir Experiments, Coefficients, and Formulas. USGS, Washington.

ISO, 2017. ISO 1438:2017. Hydrometry – Open channel flow measurement using thin-plate weirs. 3. ISO, Geneva. https://www.iso.org/standard/66463.html

King, H.W., 1916. Flow of water over right-angled V-notch weir. The Michigan Technic, 29, 3, 189–195.

Kulin, G., Compton, P.R., 1975. A guide to methods and standards for the measurement of water flow., National Bureau of Standards, Washington.

Lenz, A.T., 1942. Viscosity and surface tension effects on V-notch weir coefficients. Trans. Am. Soc. Civ. Eng., 351–374.

Mampaey, F., Xu, Z.-A., 1995. Simulation and experimental validation of mould filling. Proc. Modeling of Casting, Welding and Advanced Solidification Processes VII, London, September 10-12. https://www.osti.gov/biblio/227725

Met-Flow SA, 2020. Met-Flow UVP-DUO Profiler, Met-Flow SA, Ch. Auguste-Pidou 8, 1007 Lausanne, Switzerland, 7.

Menter, F.R., 1993. Zonal two-equation k-ω turbulence models for aerodynamic flows. AIAA Paper 93-2906. https://doi.org/10.2514/6.1993-2906

Menter, F.R., 1994. Two-equation eddy-viscosity turbulence models for engineering applications. AIAA Journal, 32, 8, 1598-1605. https://doi.org/10.2514/3.12149

Menter, F.R., Lechner, R., Matyushenko, A., 2021. Best Practice: RANS Turbulence Modeling in Ansys CFD. ANSYS.

Milburn, P., Burney, J., 1988. V-notch weir boxes for measurement of subsurface drainage system discharges. Can. Agr. Eng., 30, 2, 209–212.

Numachi, F., Hutizawa, S., 1941a. On the overflow coefficient of a right-angled triangular weir (2. Notice). J. Soc. Mech. Eng., 44, 286, 286. (In Japanese.) https://doi.org/10.1299/jsmemag.44.286_5_1

Numachi, F., Hutizawa, S., 1941b. On the overflow coefficient of a right-angled triangular weir (2. Notice). Trans. Jpn. Soc. Mech. Eng., 7, 27–3, 5–9. (In Japanese.) https://doi.org/10.1299/kikai1938.7.27-3_5

Numachi, F., Hutizawa, S., 1942a. On the overflow coefficient of a right-angled triangular weir (3. Notice). J. Soc. Mech. Eng., 45, 308, 725. (In Japanese.) https://doi.org/10.1299/jsmemag.45.308_725_2

Numachi, F., Hutizawa, S., 1942b. On the overflow coefficient of a right-angled triangular weir (3. Notice). Trans. Jpn. Soc. Mech. Eng., 8, 33–3, 37–40. (In Japanese.) https://doi.org/10.1299/kikai1938.8.33-3_37

Numachi, F., Kurokawa, T., Hutizawa, S., 1940a. On the overflow coefficient of a right-angled triangular weir. J. Soc. Mech. Eng., 43, 275, 45. (In Japanese.) https://doi.org/10.1299/jsmemag.43.275_45_2

Numachi, F., Kurokawa, T., Hutizawa, S., 1940b. On the overflow coefficient of a right-angled triangular weir). Trans. Jpn. Soc. Mech. Eng., 6, 22–3, 10–14. (In Japanese.) https://doi.org/10.1299/kikai1938.6.22-3_10

Numachi, F., Saito, I., 1948. On allowable shortest length of channel for triangular notch. J. Soc. Mech. Eng., 51, 357, 229–230. (In Japanese.) https://doi.org/10.1299/jsmemag.51.357_229_2

Numachi, F., Saito, I., 1951. On allowable shortest length of channel for triangular notch. Trans. Jpn. Soc. Mech. Eng., 17, 56, 1–3. (In Japanese.) https://doi.org/10.1299/kikai1938.17.1

OpenCFD, 2024. OpenFOAM [software]. https://www.openfoam.com/

Pospíšilík, Š., 2023. Determination of small discharges of water by triangular notch thin-plate weirs. Doctoral Thesis. Brno University of Technology, Brno. (In Czech)

Pospíšilík, Š., Zachoval, Z., 2023. Discharge coefficient, effective head and limit head in the Kindsvater-Shen formula for small discharges measured by thin-plate weirs with a triangular notch. J. Hydrol. Hydromech., 71, 1, 35–48. https://doi.org/10.2478/johh-2022-0040

Pospíšilík, Š., Zachoval, Z., Gabriel, P., 2024. Flow over thin-plate weirs with a triangular notch – influence of the relative width of approach channel with a rectangular cross-section, J. Hydrol. Hydromech., 72, 2, 199–206. https://doi.org/10.2478/johh-2024-0008.

Rezazadeh, S., Manafpour, M., Ebrahimnejadian, H., 2020. Three-dimensional simulation of flow over sharp-crested weirs using volume of fluid method. Journal of Applied Engineering Sciences, 10, 23, 75–82. https://doi.org/10.2478/jaes-2020-0012

Roache, P.J., 1994. Perspective: A Method for Uniform Reporting of Grid Refinement Studies. Journal of Fluids Engineering, 116, 405–413.

Saadatnejadgharahassanlou, H., Zeynali, R.I., Gharehbaghi, A., Mehdizadeh, S., Vaheddoost, B., 2020. Three dimensional flow simulation over a sharp-crested V-notch weir. Flow Measurement and Instrumentation, 71, 101684. https://doi.org/10.1016/j.flowmeasinst.2019.101684

Schoder, E.W., Turner, K.B., 1929. Precise weir measurements. Trans. Am. Soc. Civ. Eng., 1929, 93, 999–1190.

Shen 1981: Shen, J., 1981. Discharge characteristics of triangular-notch thinplate weirs: Studies of flow of water over weirs and dams.Geological survey water-supply paper, 1617-B. U. S. Govern-ment Printing Office, Washington.

Sinclair, J.M., Venayagamoorthy, S.K., Gates, T.K., 2022. Some insights on flow over sharp-crested weirs using computational fluid dynamics: Implications for enhanced flow measurement. J. Irrig. Drain Eng., 148, 6, 04022011. https://doi.org/10.1061/(ASCE)IR.1943-4774.0001652

Streeter, V.L., 1942. The kinetic energy and momentum correction factors for pipe and for open channels of great width, Civil Engineering, 12, 4, 212–213.

Strickland, T.P., 1910. Mr. James Barr's experiments upon the flow of water over triangular notches. Engineering, 90, 598.

Subramanya, K., 2019. Flow in Open Channels. 4. McGraw Hill, New Delhi. ISBN 978-9353166298.

Thomson, J., 1858. On experiments on the measurement of water by triangular notches in weir boards. In: Proc. Twenty-eight Meeting of the British Association for the Advancement of Science. John Murray, Albemarle Street, London, 181–185.

Thomson, J., 1861. On experiments on the gauging of water by triangular notches. In: Proc. Thirty-first Meeting of the British Association for the Advancement of Science. John Murray, Albemarle Street, London, 151–158.

Van Maele, K., Merci, B., 2006. Application of two buoyancy-modified k-ε turbulence models to different types of buoyant plumes. Fire Saf. J. 41, 122–138. https://doi.org/10.1016/j.firesaf.2005.11.003

White, F.M., 2011. Fluid Mechanics. 7th ed. McGraw Hill, New York. ISBN 978-0-07-352934-9

Yakhot, V., Orszag, S.A., 1986. Renormalization group analysis of turbulence I. Basic theory. Journal of Scientific Computing, 1, 1, 3–51. https://doi.org/10.1007/BF01061452

Yarnall, D.R., 1912. The V-notch weir method of measurement. J. Am. Soc. Mech. Eng., 34, 2, 1479–1494.

Yarnall, D.R., 1927. Accuracy of the V-notch-weir method of measurement. Trans. Am. Soc. Mech. Eng., 48, 939–964.

Zachoval, Z., Roušar, L., 2015. Flow structure in front of the broad-crested weir. In EPJ Web of Conferences 92, 02117. https://doi.org/10.1051/epjconf/20159202117

Received 16 December 2024
Accepted 24 March 2025